

This item is the archived peer-reviewed author-version of:

Exploring the oxidative mechanisms of bitumen after laboratory short- and long-term ageing

Reference:

Pipintakos Georgios, Soenen Hilde, Ching Hong Yue Vincent, Vande Velde Christophe, Van Doorslaer Sabine, Lemièr Filip, Varveri Aikaterini, Van den bergh Wim.- Exploring the oxidative mechanisms of bitumen after laboratory short- and long-term ageing
Construction and building materials - ISSN 0950-0618 - 289(2021), 123182
Full text (Publisher's DOI): <https://doi.org/10.1016/J.CONBUILDMAT.2021.123182>
To cite this reference: <https://hdl.handle.net/10067/1770690151162165141>

Exploring the oxidative mechanisms of bitumen after laboratory short- and long-term ageing

Georgios Pipintakos ^{a,*}, Hilde Soenen ^b, H.Y. Vincent Ching ^c, Christophe Vande Velde ^d, Sabine Van Doorslaer ^c, Filip Lemièrè ^e, Aikaterini Varveri ^f and Wim Van den bergh ^a

^a University of Antwerp, EMIB research group, Groenenborgerlaan 171, Antwerp 2020, Belgium

^b Nynas NV, Groenenborgerlaan 171, Antwerp 2020, Belgium

^c University of Antwerp, BIMEF research group, Universiteitsplein 1, Wilrijk 2610, Belgium

^d University of Antwerp, iPRACS research group, Groenenborgerlaan 171, Antwerp 2020, Belgium

^e University of Antwerp, BAMS research group, Groenenborgerlaan 171, Antwerp 2020, Belgium

^f Delft University of Technology, Pavement Engineering, Stevinweg 1, Delft 2628 CN, Netherlands

* Corresponding author : georgios.pipintakos@uantwerpen.be

1 Abstract

2 Understanding the fundamental mechanisms of oxidative ageing in bitumen is considered of paramount importance in
 3 order to take steps towards durable binders able to tackle distresses related to this phenomenon which deteriorates the
 4 asphalt performance. This paper focuses on the identification of the intermediate and final oxygenated products after
 5 short- and long-term laboratory ageing simulated with rolling thin-film oven testing (RTFOT) and pressurised ageing
 6 vessel (PAV) respectively. Three binders were investigated in this study, two originated from the same wax-free crude
 7 source, while the third was obtained from a different source, containing natural wax, and followed a different
 8 manufacturing process. Fourier-Transform Infrared (FTIR) spectroscopy demonstrated a clear increase of the
 9 sulfoxide and carbonyl functional groups upon ageing for all the binders independently of origin, manufacturing or
 10 performance. Electron Paramagnetic Resonance (EPR) spectroscopy showed an increase of the organic carbon-centred
 11 radicals after short-term ageing (RTFOT), whereas after PAV these radicals remained constant in the two wax-free
 12 binders originating from the same crude source, and even decreased for the third, waxy binder. Proton Nuclear
 13 Magnetic Resonance (¹H-NMR) spectroscopy reported differences in the relative distribution of protons between the
 14 binders in the unaged state, and similar minor changes after both ageing steps regardless of the binder's crude source
 15 and distillation. The results of Time-of-Flight Secondary Ion Mass Spectrometry (TOF-SIMS) revealed that SO_x- and
 16 (OH)_x-containing compounds are produced after the sequentially occurring short- and long-term ageing in both wax-
 17 free bitumens, whereas an almost constant behaviour of aliphatics after PAV ageing can be seen for the same bitumens.
 18 Finally, the strengths and weaknesses of each of these experimental techniques were reviewed and compared versus
 19 the obtained results and possible ageing mechanisms.

20 Highlights:

- 21 • The oxidative mechanisms in bitumen were studied after laboratory short- and long-term ageing.
- 22 • Three binders of varying crude source, distillation, performance and wax presence were investigated.
- 23 • ¹H-NMR demonstrated slight changes in the relative proton distribution upon ageing.
- 24 • EPR supported an increase of organic carbon-centred radicals after short-term ageing.
- 25 • TOF-SIMS revealed an increase of SO_x-, (OH)_x-containing compounds because of ageing.

26 **Keywords:** bitumen; EPR; ¹H-NMR; TOF-SIMS; FTIR; ageing; oxidative mechanisms

27 1. Introduction

28 Bitumen is one of the main components of asphalt pavements and consists of a vast number of organic molecules [1].
29 Due to its organic constituents bitumen is prone to oxidation during exposure to mixing and environmental conditions
30 [2]. Albeit other irreversible physicochemical processes take place in bitumen (volatilisation and condensation), oxidative
31 ageing is considered of utmost importance since it generally deteriorates the pavement performance [3,4]. To date, a lot
32 of studies have already demonstrated this negative impact of oxidative ageing resulting in the brittleness of bitumen
33 responsible for several distresses in asphalt scale such as cracking and ravelling [5–8]. However, it should be noted that
34 moderated ageing may indicate also positive effects in pavement if one is able to control it, *i.e.* by reducing severe
35 deformations and rutting.

36 Since the chemical structure of bitumen is complex and also changes as a result of oxidative ageing, it has become
37 apparent how crucial the understanding of bitumen chemistry is [9]. The bitumen's exact composition depends on the
38 refinery process and the origin of crude oil, a fact that makes the determination of bitumen chemistry even more
39 challenging [10,11]. Despite these difficulties, it has been proposed that the reaction mechanisms in each bitumen follow
40 two-rate determining oxidation phases: the chemically distinct fast and slow phases [6,12,13]. Initiated by Petersen and
41 his coworkers, recent literature confirmed experimentally the formation of organic carbon-centred radicals, which would
42 be expected in a dual-sequential oxidation scheme [12,14]. The existence of free radicals will most likely provoke the
43 chemical reactions resulting eventually in the formation of polar sulfoxides from non-polar sulfides and polar ketones (as
44 well as anhydrides and carboxylic acids in smaller amounts) from benzylic carbon moieties [9].

45 Hitherto, isothermal reaction kinetic studies revealed also differences in the reaction rate and the formation of the two
46 major oxidation products, namely carbonyls and sulfoxides [15]. Moreover, high temperatures, above 120 °C may cause
47 thermal decomposition of the sulfoxides [13,16] and as such better insights into the sequential two-phase mechanism are

48 needed since, in reality, the temperature varies between the different stages of the service life. It is important to note that
49 during service life extreme temperatures greater than 80 °C are never reached, while the temperatures during the paving
50 stages depend on the asphalt mixture application (hot, warm, cold).

51 It has long been speculated that certain oxidation products correlate well with the viscosity of bitumen [6,17]. Previous
52 research highlighted additionally that the effect of temperature during the production stage, responsible for the short-term
53 ageing, is more crucial for the intensity of the main oxidation products than the temperature during service life, associated
54 with the long-term ageing of bitumen [18,19]. The effect of ageing time of each stage is considered also crucial for the
55 end products and the bitumen's rheological behaviour. Moreover, to realistically capture the main products formed upon
56 ageing as well as the role of intermediate products and organic radicals, one should go beyond isothermal kinetics. Ideally,
57 taking also into account the effect of mineral fillers in the composition has been considered to be a more precise
58 approximation of field ageing [20], although the interactions between the components yet remain to be understood.

59 In order to mimic in-situ changes of bitumen due to oxidation, a common practice is to utilise routine tests simulating
60 the short- and long-term ageing. More specifically, the rolling thin film oven test (RTFOT) [21] followed by the
61 pressurised ageing vessel (PAV) [22] are most commonly used to simulate the elevated temperature during production
62 and paving and the weather conditions during use-life respectively. According to literature conditioning in PAV of 20
63 hours at a pressure of 2.1 MPa corresponds to 7-10 years of field ageing for base layers [23–25], where the exact
64 equivalence depends on the bitumen and type of the asphalt mixture (dense, porous, etc.). However, controversy exists
65 whether the high temperatures and pressure employed in artificial ageing can adequately capture the changes from a
66 chemical perspective as the chemical mechanisms, in reality, may be somewhat different [9,26]. For example, the
67 exposure to ultraviolet radiation or the incorporation of reactive oxygen species in the atmosphere can alter considerably
68 the overall chemical routes or concentration of oxygenated products during ageing [27,28].

69 Of pragmatic importance is to examine whether the artificial ageing simulations, widely used in the asphalt sector,
70 account for a fair correspondence with the ageing mechanisms reported previously in kinetic studies [12,15,29]. A
71 fundamental understanding of bitumen oxidation is considered crucial for the implementation of the appropriate modifiers
72 or rejuvenators when recycling and the reviewing of the protocols for artificial ageing, in order to adapt them in a
73 controlled manner. Last but not least, taking steps towards the partial or complete prevention of oxidation in asphalt will
74 bridge the gap between the depletion of an organic, non-renewable material, like bitumen, and a universal policy
75 promoting long-lasting pavements and sustainability.

76 Given that the molecular interactions and chemical composition affect primarily the ability of molecules to flow and
77 consequently the rheological behaviour of bitumen [4,30–32], an in-depth inspection of the underlying mechanisms after

78 standardised simulations is thus considered more than crucial. This study aims primarily to identify the basic ageing
 79 compounds formed after artificial ageing. Specifically, the proposed approach employs advanced spectroscopy (FTIR,
 80 EPR, ¹H-NMR and TOF-SIMS) in an attempt to capture the structural and chemical changes upon ageing with routine
 81 laboratory tests. This work aims finally at accounting for the effect of both the crude source, the binder's penetration
 82 grade and the distillation process on the mechanisms upon standardised ageing.

83 **2. Materials and methods**

84 **2.1. Materials**

85 The bituminous binders selected for this work vary with regard to the penetration grade, origin of the crude oil and
 86 refinery process. Bitumen A and B are straight-run binders, originating from the same acidic, wax-free crude with a
 87 penetration grade of 10/20 and 160/200 respectively. A third binder C of a different crude source with similar penetration
 88 to binder B was also examined, however, this binder was the result of a thermal cracking process (visbreaking) and it
 89 contained natural wax (crystallisable compounds). The wax presence was identified via Differential Scanning Calorimetry
 90 measurements and revealed a melting enthalpy of 9.6 J/g. The empirical properties of all binders are summarised in Table
 91 1.

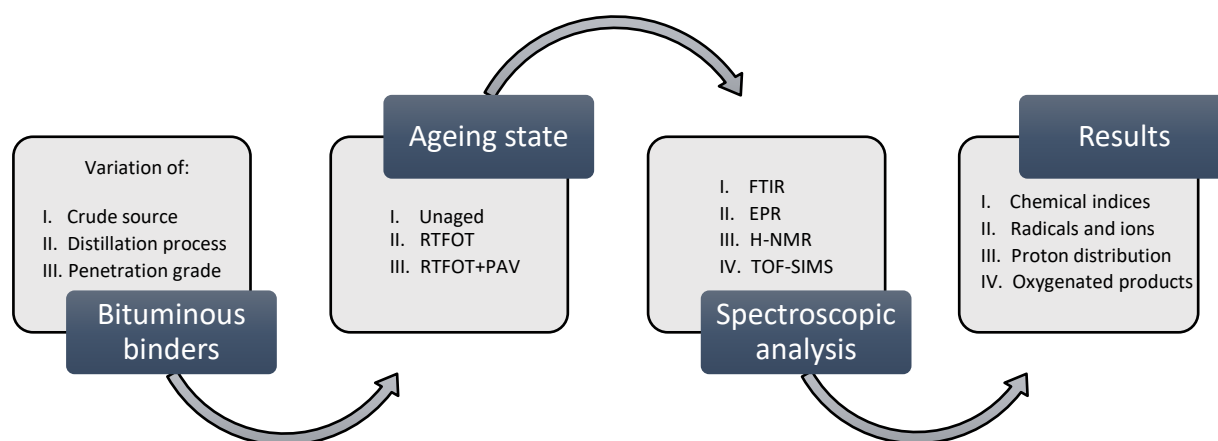
92 Table 1: Empirical properties of the bituminous binders in the unaged state.

Material	Property	Binder			Test Method
		A	B	C	
Bitumen	Penetration 25 °C (0.1 mm)	16	189	190	EN1426
	Softening point (°C)	61.1	37.5	39.2	EN1427
	Penetration index, Ip	-1.06	-1.46	-0.63	EN12591
	Performance grade	76-16	52-28	52-22	AASHTO MP 1

93 **2.2. Ageing simulations**

94 The oxidative ageing in the lab was simulated for the short term-ageing by the rolling thin film oven test (RTFOT)
 95 according to EN 12607-1 [21] and for the long-term ageing with the pressurised ageing vessel (PAV) according to EN
 96 14769 [22]. Typically for RTFOT, 35 grams of unaged virgin bitumen are placed in each bottle inside a rotating carousel
 97 for 75 minutes, where temperature and fresh air flow are set at 163 °C and 4 L/min. This test simulates the high
 98 temperatures occurring during the production and is linked with the initial fast-rate oxidation phase of a dual-sequential
 99 oxidation scheme. The PAV protocol, on the other hand, was followed for all the short-term aged samples after RTFOT,
 100 in an attempt to reproduce in a short period of time the effect of many years in the field. The PAV procedure requires 50
 101 grams of bitumen to be placed in pans inside a pressure chamber, which results in a thin film of bitumen able to be
 102 sufficiently aged. In the current study, the temperature was set at 100 °C with an air pressure of 2.1 MPa for a total duration
 103 of 20 hours.

104 In order to simplify the nomenclature for each ageing state of the three binders, the following code 'X-ageing state'
 105 indicates the type of binder X (A, B or C) and the ageing state (Unaged, RTFOT or PAV). After applying the ageing
 106 conditions, appropriate samples were prepared for each spectroscopic technique described in the following subsection.
 107 For the ease of the reader, a graphical summary with the expected outcomes by each analysis is provided in Figure 1.



108 Figure 1: Research methodology

109 2.3. Spectroscopic techniques

110 2.3.1. Attenuated Total Reflectance-Fourier Transform Infrared (ATR-FTIR)

111 For all the ageing states of each bitumen at least three individual samples were analysed using a Thermo Scientific
 112 Nicolet iS10 FTIR spectrometer equipped with an Attenuated Total Reflectance (ATR) fixture (diamond crystal) and a
 113 Smart Orbit Sampling Accessory. For the sample preparation, metal cans containing the bituminous materials were heated
 114 in an oven at 155 °C for 20 minutes. This time and temperature were found to be sufficient for all the used bitumens and
 115 ageing states to obtain a liquid sample which was afterwards stirred for 1 minute and a single droplet was placed on the
 116 diamond FTIR crystal, after a background spectrum acquisition. The droplet was allowed to cool down for 5 minutes.
 117 The spectra were recorded as the average of 32 repetitive scans, at a resolution of 4 cm⁻¹, in a wavenumber band ranging
 118 from 400 cm⁻¹ to 4000 cm⁻¹. The analysis of the spectrum involves the calculation of band-areas in certain peaks from
 119 which chemical indices with regard to ageing of bitumen and its structural fingerprint can be derived. The reader is
 120 referred to the protocol given in [33] and to the calculation of the areas with their wavelength limits and corresponding
 121 bond vibrations in [12]. The indices that can be extracted by making use of these areas are given in Equations 1-4. Example
 122 spectra of bitumen A in the three ageing states are given in Figure 2.

$$\text{Sulfoxide index} = \frac{A_{1030}}{\sum^n A_n} \quad (1)$$

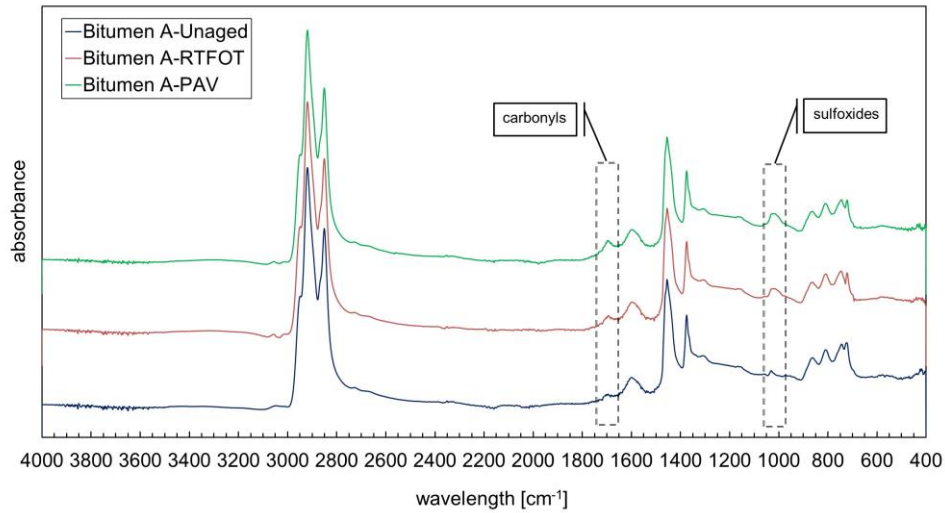
$$\text{Carbonyl index} = \frac{A_{1700}}{\sum^n A_n} \quad (2)$$

$$\text{Branched aliphatic index} = \frac{A_{1376}}{A_{1460} + A_{1376}} \quad (3)$$

$$\text{Aromaticity index} = \frac{A_{1600}}{\sum^n A_n} \quad (4)$$

123

where $n = 724, 743, 814, 864, 1030, 1376, 1460, 1600, 1700, 2862, 2953$



124

125

Figure 2: Example of FTIR spectra in all the ageing states of bitumen A with the main oxygenated functional groups.

126 2.3.2. Electron Paramagnetic Resonance (EPR)

127 For the identification of the organic radicals and metal ions, continuous-wave (CW) EPR spectra of the three binders
 128 in all the ageing states were acquired with a Bruker Elexsys E680 (X/W) spectrometer equipped with an ER 4102ST
 129 TE102 mode resonator at 9.75 GHz (X-band). Three replicates for each ageing state and each binder were placed inside
 130 propylene Eppendorf tubes and the exact masses were measured priorly in order to normalise the number of spins per
 131 gram for each detected paramagnetic component. It was found that all the recorded spectra include contributions of a
 132 vanadyl centre (VO^{2+} , $S = 1/2$) and an organic carbon-centred radical. The protocol described previously in [12] was
 133 followed here. Briefly, in a preliminary study the effects of power saturation were assessed and for all the subsequent
 134 measurements a microwave power of 0.5 mW, a centre magnetic field at 341 mT and sweep width of 20 mT, resolution
 135 of 2048 points, a modulation amplitude of 0.1 mT and a modulation frequency of 100 kHz over 2 scans, was selected.
 136 The spectra were next simulated with the EasySpin-6.0 module [34] in Matlab2018b from which the EPR parameters
 137 (given in [12]) of the two species and the relative amount of spins between them can be derived. The VO^{2+} centres were
 138 attributed to VO^{2+} porphyrin centres found in heavy crude oils [35,36] while the second signal was assigned to carbon-
 139 based organic radicals [37]. Quantification of the corresponding number of spins was obtained by comparison of the

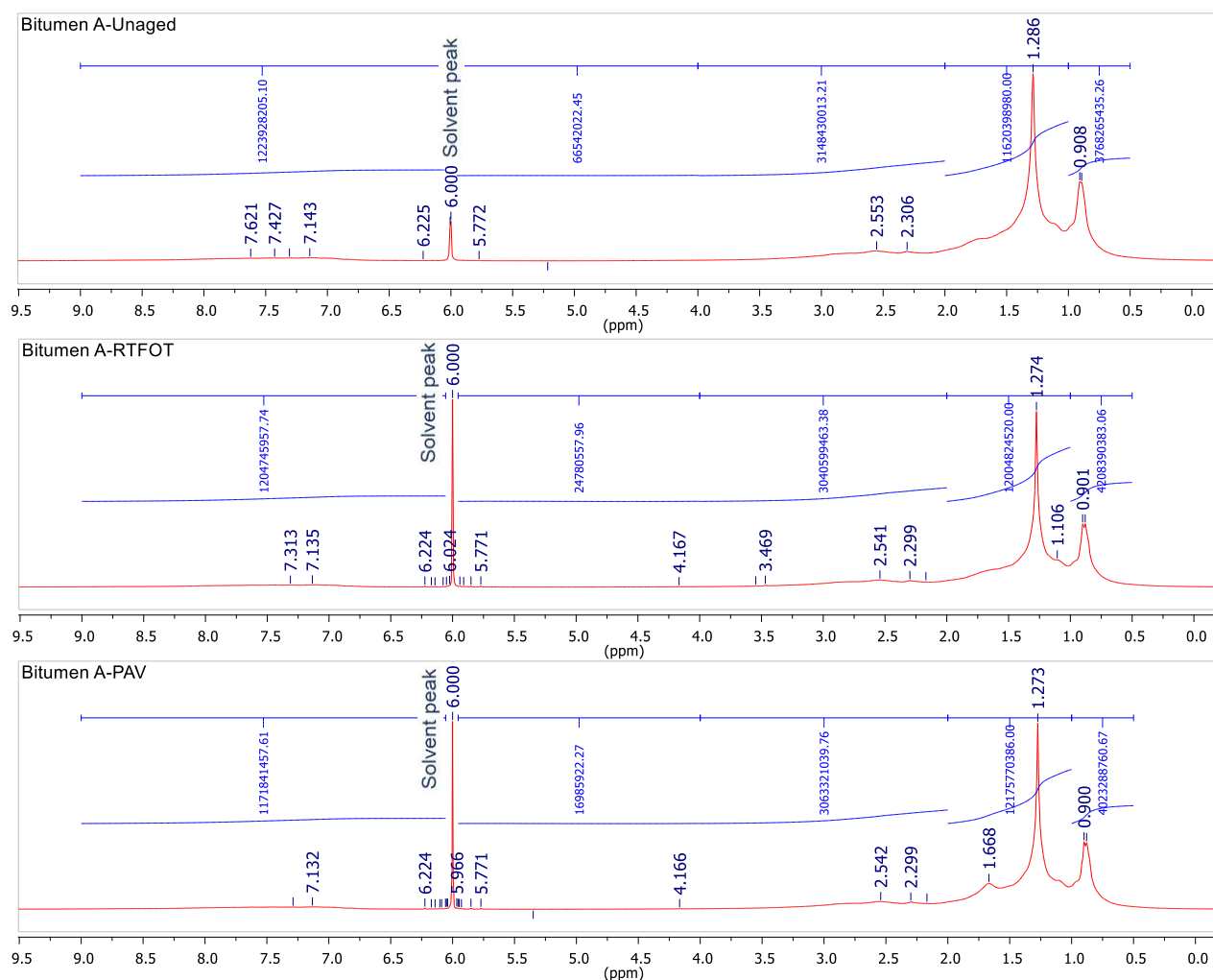
140 double integral of the spectra with standard curve derived using different concentrations of TEMPO (2,2,6,6-tetramethyl-
141 1-piperidinyloxy) in toluene.

142 2.3.3. Proton Nuclear Magnetic Resonance ($^1\text{H-NMR}$)

143 $^1\text{H-NMR}$ is a superior spectroscopic technique able to characterise the molecular structure of a material, even for a
144 complex one, such as bitumen. It can assist with the characterisation of the relative amount of different types of aliphatic
145 olefinic and aromatic protons in bitumen [38,39] and therefore can also be applied to capture the proton distribution upon
146 ageing in bitumen. Data collection of all the bituminous binders at room temperature was conducted with a high-resolution
147 liquid-state Bruker Avance III HD 400 MHz smart probe spectrometer (32 scans). Preliminary measurements with CDCl_3
148 (deuterated chloroform) as solvent showed interference with the aromatic region signal of bitumen, while different
149 concentrations of dissolution with 5 and 40 mg of bitumen showed a poor and an overloaded $^1\text{H-NMR}$ signal respectively.
150 Therefore, about 20 mg of bitumen were dissolved in 650 μl of deuterated tetrachloroethane ($\text{C}_2\text{D}_2\text{Cl}_4$) inside borosilicate
151 NMR tubes (ASTM Type 1 Class B glass) of diameter 5 mm and a wall thickness of 0.4 mm. To ensure an adequate
152 dissolution of the solvent with the specimen all vials containing the dissolved samples were additionally placed inside an
153 ultrasonic water bath before the $^1\text{H-NMR}$ analysis. The repeatability was provided by means of standard deviations. After
154 the analysis, steps were first taken to accurately calibrate the starting chemical shift based on the difference of the residue
155 solvent peak (6.00 ppm) with respect to TMS (tetramethylsilane) (0.00 ppm) [40]. The analysis of the results was
156 performed in the MestreNova spectral analysing software following the integration of the typical proton chemical shift
157 regions reported in [41], neglecting each time the protons associated to heteroatoms and the residue solvent at 6.00 ppm.
158 The latter study classifies a typical $^1\text{H-NMR}$ spectrum of bitumen in five main groups given in Table 2. Normalisation of
159 all the integrated areas with the exact sample mass allows for a fair comparison of the relative percentage distribution of
160 the different type of protons identified in bituminous samples. The normalised per mass areas were also inspected and
161 same trends with the relative percentage distribution were followed, therefore the latter was chosen for the analysis of
162 this study. Figure 3 illustrates examples of spectra of bitumen A in all ageing states with the normalised per sample mass
163 area integrations.

164 Table 2: Typical groups of protons in bitumen [41].

Designation	Chemical shift range	Type of protons	Major proton peak in this region
H_{methyl}	0.5-1.0	Aliphatic hydrogen on C_γ and the CH_3 beyond the C_γ to aromatic rings	Methyl
$\text{H}_{\text{methylene}}$	1.0-2.0	Aliphatic hydrogen on C_β and the CH_2 beyond the C_β to aromatic rings	Methylene
$\text{H}_{\alpha\text{-alkyl}}$	2.0-4.0	Aliphatic hydrogen on C_α to aromatic rings	-
$\text{H}_{\text{olefinic}}$	4.0-6.0	Olefinic hydrogen	-
$\text{H}_{\text{aromatic}}$	6.0-9.0	Aromatic hydrogen	-



165 Figure 3: Example of ¹H-NMR spectra in all the ageing states of bitumen A with their main proton peaks.

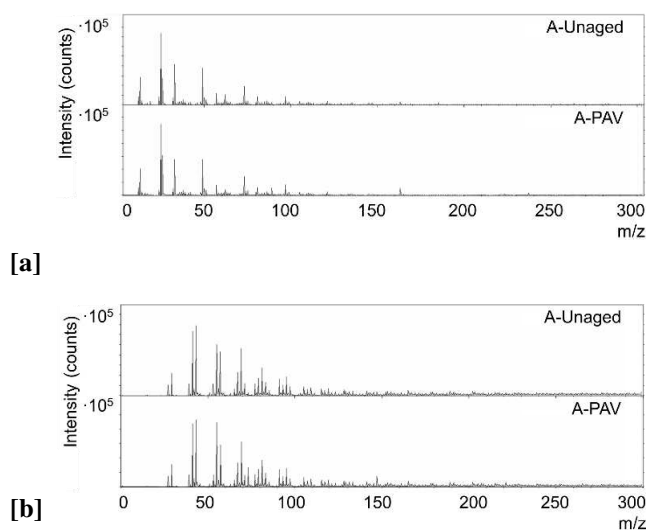
166 2.3.4. Time-of-Flight Secondary Ion Mass Spectrometry (TOF-SIMS)

167 A TOF-SIMS IV spectrometer (ION-TOF GmbH) was utilised in this study, with the ultimate goal to unwrap the
 168 molecular structure of the products formed upon complete oxidation at the surface of bituminous samples. A bismuth
 169 liquid metal ion gun was used for bombarding the surface of bituminous samples with 25 keV Bi₃⁺ primary ions. The
 170 secondary ions emitted from the surface were separated based on the mass-to-charge ratio (m/z) by the TOF analyser
 171 [42]. Mass spectra were recorded up to m/z 1270. Charging of the sample was compensated using the electron flood gun.
 172 The instrument was controlled and data acquired by the IONVAC software (IonTOF). The data were processed using
 173 Surfacelab 7 (IonTOF).

174 Following the procedure for conditioning of the samples described in [12,43] the temperature of the sample in the ion
 175 source was maintained between -50 and -80 °C using liquid nitrogen, in order to avoid diffusion/segregation in the vacuum
 176 system. Silicon wafers of dimensions 10 mm x 10 mm were used as substrates for the three bituminous binders in both

177 the unaged and PAV ageing condition. Spectra of positive and negative ions were recorded at three different spots per
 178 sample in analysis areas of 500 μm x 500 μm with a high mass resolution of 2000 $\text{m}/\Delta\text{m}$. All the samples were treated
 179 prior to analysis with exactly the same protocol described elsewhere in [43] to obtain flat bituminous films of
 180 approximately 1 mm. The spectra for all the samples were analysed based on the intensity of the areas of selective mass-
 181 to-charge-ratios, assigned to specific ions (Table 3), normalised by the total recorded ions' intensity (counts). Example
 182 spectra of bitumen A of positive and negative ions are given in Figure 4.

183 Table 3: Utilised negative and positive oxygenated ion fragments.



Ion	Observed mass (m/z)	Assignment of molecular structure
OH^-	17.003	$(\text{OH})_x$ -containing
C_2OH^-	41.005	$(\text{OH})_x$ -containing
CHSO^-	60.974	SO_x -containing
$\text{C}_2\text{H}_3\text{SO}^-$	74.989	SO_x -containing
C_6HO^-	89.001	$(\text{OH})_x$ -containing
C_3H_7^+	43.055	Aliphatic
C_4H_7^+	55.054	Aliphatic
C_4H_9^+	57.070	Aliphatic
C_5H_7^+	67.049	Aliphatic
C_5H_9^+	69.068	Aliphatic
$\text{C}_5\text{H}_{11}^+$	71.088	Aliphatic
C_6H_9^+	81.065	Aliphatic
$\text{C}_6\text{H}_{11}^+$	83.085	Aliphatic
$\text{C}_6\text{H}_{13}^+$	85.104	Aliphatic
$\text{C}_7\text{H}_{11}^+$	95.079	Aliphatic
$\text{C}_7\text{H}_{13}^+$	97.102	Aliphatic
C_9H_7^+	115.033	Aromatic
$\text{C}_{10}\text{H}_8^+$	128.036	Aromatic
$\text{C}_{13}\text{H}_9^+$	165.035	Aromatic

184 Figure 4: Example of negative [a] and positive [b] TOF-SIMS ion spectra
 185 of bitumen A in the unaged state and after PAV.

186 2.3.5. Experimental challenges

187 Although the techniques used in this study are robust enough, limitations may still exist, especially when investigating
 188 a multi-component mixture like bitumen. This needs to be acknowledged when reviewing and comparing the findings of
 189 each of the techniques as the results may be contradictory.

190 First of all, FTIR-ATR and TOF-SIMS are in fact both surface analysis methods with different penetration depths, of
 191 a maximum of 2-3 micrometres for FTIR-ATR [44], and only a few nanometres for TOF-SIMS [42]. In TOF-SIMS an
 192 air-cooled surface is investigated, while in FTIR-ATR, the interface as formed against the ATR diamond crystal is
 193 investigated. In literature, it has been demonstrated that bitumen may exhibit a different composition depending on the
 194 substrate and the environment [43,45,46]. Especially, the reproducibility of TOF-SIMS results is an issue that needs
 195 special care as the exact film thickness and flatness may affect the obtained spectra. In the current study the preparation
 196 procedure, the thermal history of the binders and the control of film thickness was kept constant, with the latter calculated
 197 by the exact amount of binder used on the substrate.

198 Secondly, sample preparation and sample thermal history are different for both the FTIR and TOF-SIMS tests: in FTIR
199 a small hot drop is placed directly onto the crystal and tested. In TOF-SIMS, hot bitumen drops are first placed on a
200 substrate, which is then shortly reheated and air-cooled, to achieve a flat surface. The analysis temperature is much lower
201 in TOF-SIMS compared to the other techniques, which could for example influence the extent of crystallisation of the
202 waxy bitumen compounds. For the ¹H-NMR tests, the bitumen is dissolved in deuterated tetrachloroethane, and although
203 several steps were taken to obtain dissolved samples (*i.e.* a solvent with appropriate solubility, ultrasonic bath and visual
204 inspection), there is still a risk of some undissolved species.

205 Moreover, the detection sensitivity for various chemical compounds is dependent on the respective technique, *i.e.*
206 FTIR is very sensitive to capture basic oxygenated products (carbonyls and sulfoxides) while it is rather insensitive to
207 changes such as a further aromatisation process [47]. Additionally, in TOF-SIMS only the charged species formed (and
208 not the neutral ones) after a chemical bombardment on the surface are detected. The ¹H-NMR by definition will only
209 capture hydrogenated compounds, while CW EPR shows both bulk and surface paramagnetic centres. The spectral
210 intensity will depend on the time after generation of the radicals and as such centres that are too short living will not be
211 detected in the EPR experiment.

212 Finally, the ageing tests, which are the standard ageing protocols when investigating bitumen, are not conducted in a
213 closed system; so there is a possibility that volatiles, present or formed during ageing may leave the sample. This effect
214 would be the same for all the analyses performed on the sample after the ageing tests.

215 **3. Results and discussion**

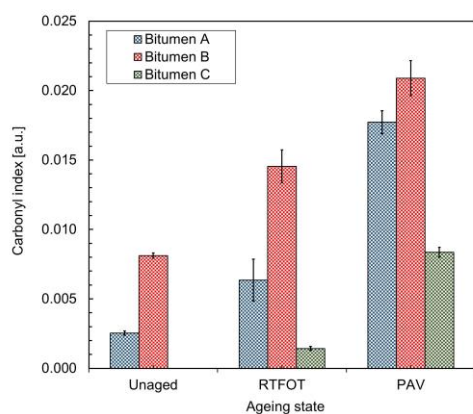
216 **3.1.1. FTIR analyses**

217 The indices presented in Equations 1-4 were determined for the three bitumens under investigation before and after
218 laboratory short and long-term ageing. The results are consistent with the view that an increase with ageing severity is
219 observed after standardised ageing for the main oxidative indices, namely the sulfoxide and the carbonyl index [48,49].
220 Figures 5 and 6 depict the evolution of the two indices and the effect of each ageing state is discussed herein in percentage
221 increase of the virgin state.

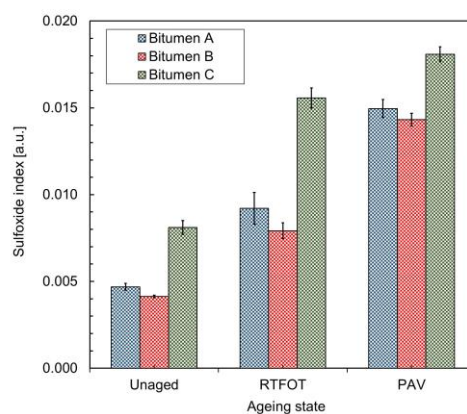
222 A relative comparison of the formation rates is performed in terms of percentage differences. The results of bitumen
223 A for the carbonyl index show an increase of 150.7% and 600.1% after RTFOT and PAV respectively, which indicates a
224 more rapid and steep increase compared to bitumen B (79.2% and 157.5%) which differed only in penetration grade
225 (Figure 5). The presence of carbonyl groups for these two bitumens in the unaged state can be explained by the acidic
226 nature of the crude oil from which they originated. On the contrary, for bitumen C-Unaged, a negligible initial carbonyl
227 index was obtained based on the same analysis procedure. As such percentage differences are meaningless for bitumen C

228 after RTFOT (with an initial unaged index equal to zero), but an increase in carbonyls after RTFOT ageing is clear. The
 229 significant increase of carbonyls is apparent in bitumen C after PAV which increased (484.7%) compared in this case
 230 with the index in RTFOT. Therefore, it can be speculated that the cumulative carbonyl formation rate was even faster for
 231 bitumen C than A, although a numerical straight-forward comparison of the percentage increase cannot be performed.

232 A detailed inspection of the initial sulfoxide index for C-Unaged implies that this is significantly higher than for
 233 bitumen A and B. Concerning the sulfoxide index the three bitumens show similar percentage increase after RTFOT (A-
 234 95.3%, B-91.4% and C-91.9%). The effect of the bitumen type seems to be very small on the sulfoxide formation rate
 235 after short-term ageing but after PAV ageing the sulfoxide indices increase more for bitumens A and B (A-218.9%, B-
 236 246.0%) compared to the increase of the sulfoxide index of bitumen C (123.1%).



237 Figure 5: Evolution of carbonyl index with ageing.

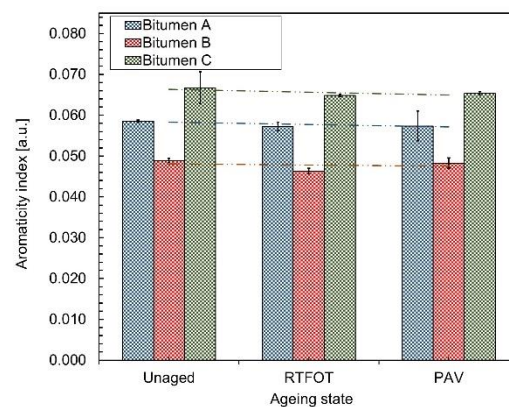
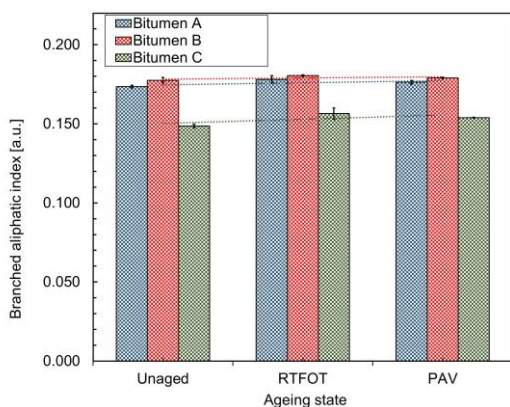


238 Figure 6: Evolution of sulfoxide index with ageing.

238 Overall, the bitumen type has little effect on the sulfoxide formation rate but seems to affect the carbonyl formation
 239 differently. On the other hand, straight-run bitumens from the same crude show a similar increase of sulfoxide upon
 240 ageing in the lab, with hard bitumen A exhibiting a more rapid carbonyl increase compared to bitumen B.

241 The representative indices for the aromatisation of bitumen were also investigated in this work. In the past, it has been
 242 assumed that aromatisation increases primarily the planarity of perhydroaromatic rings in the fast-rate reaction but it can
 243 also cause the aromatisation of alkyl-substituted naphthenic rings during the slow-rate phase [9,50]. Moreover, an
 244 interplay between the formation of aromatic structures and a reduction of aliphatics (occurring in a lesser amount) can be
 245 hypothesised, which would result in a mutual change of the aromaticity and the branched aliphatic index. Surprisingly in
 246 this study, the FTIR indices related to these compounds were constant for both the aromaticity and branched aliphatic
 247 index in all the ageing states (Figures 7 and 8). It was postulated that FTIR was not sensitive enough to capture changes
 248 related to aromatisation. Moreover, alcohol regions around $3200\text{-}3500\text{ cm}^{-1}$, seem not to be affected by ageing for all the

249 bitumens, whereas an overlap in the C-O stretch of possible alcohol formation could exist with the sulfoxide increase in
 250 the FTIR spectra. For that reason, other tests were applied as shown in the next sections.



251 Figure 7: Branched aliphatic index in all the ageing states.

Figure 8: Aromaticity index in all the ageing states.

252 3.1.2. EPR analyses

253 The evolution of the organic carbon-centred radicals and the VO^{2+} species after routine laboratory ageing simulations
 254 is given in Figures 9 and 10 respectively. Overall, the carbon-centred organic radicals showed an increase after short
 255 term-ageing with RTFOT for all the three bitumens of this work with a significant drop in the number of spins for bitumen
 256 C observed upon PAV. Bitumen A and B kept a constant number of spins of carbon-centred organic radicals between
 257 short- and long-term ageing. A previous kinetics' study suggested that the oxygen-centred radicals, such as $\bullet OH$, may
 258 abstract protons attached to benzyl rings and could yield to carbon-centred radicals [12]. The point at which the plateau
 259 of this type of radicals appears is considered as the onset of the slow-rate phase. Hence, the differences of bitumen A, B
 260 and C suggest that the intermediate products, such as the organic carbon-based radicals, are affected differently by ageing.
 261 Furthermore, the different initial higher number of organic radical spins in bitumen C is possibly related to the visbreaking
 262 process of this bitumen.

263 When it comes to the VO^{2+} centres, identified with the EPR analyses, the present study for these metal ions confirms
 264 earlier studies [12], namely that these centres remain in general unaffected by the oxidation process, as it is evidenced by
 265 the stabilisation of the number of spins in all the ageing states (Figure 10). The present article raises a significant point
 266 about a possible correlation of the vanadyl species and the vanadium content, present in bitumen's composition since it
 267 can be exploited as an indicator and marker of the origin following [51].

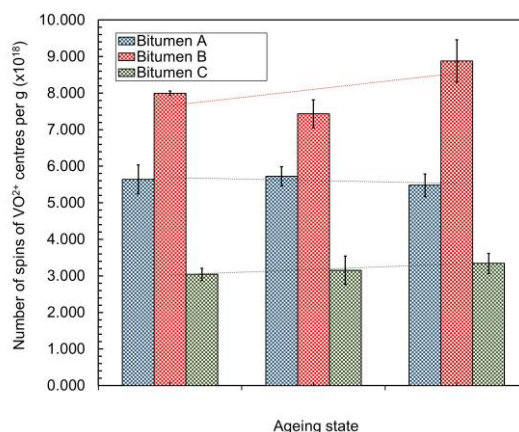
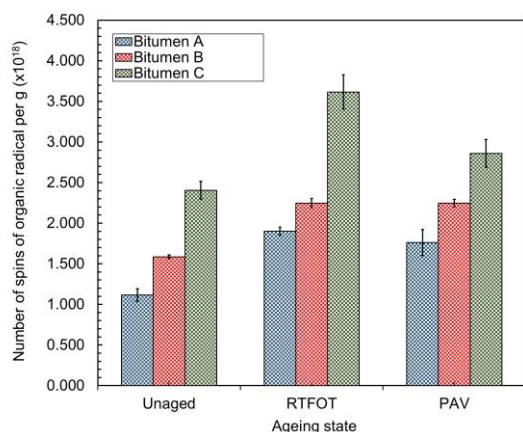


Figure 9: Evolution of carbon-centred radicals in all the ageing states. Figure 10: Evolution of VO²⁺ centres in all the ageing states.

268 Up to this point, the differences between bitumen C and bitumens A and B may affect the initial number of spins of
 269 organic radicals in the unaged state. The different penetration grade between bitumen A and B implies also that the
 270 distillation grade of the same crude oil may have an effect on the VO²⁺ centres with the softer bitumen B presenting the
 271 higher number of VO²⁺ spins.
 272

273 3.1.3. ¹H-NMR analyses and proton relative distribution

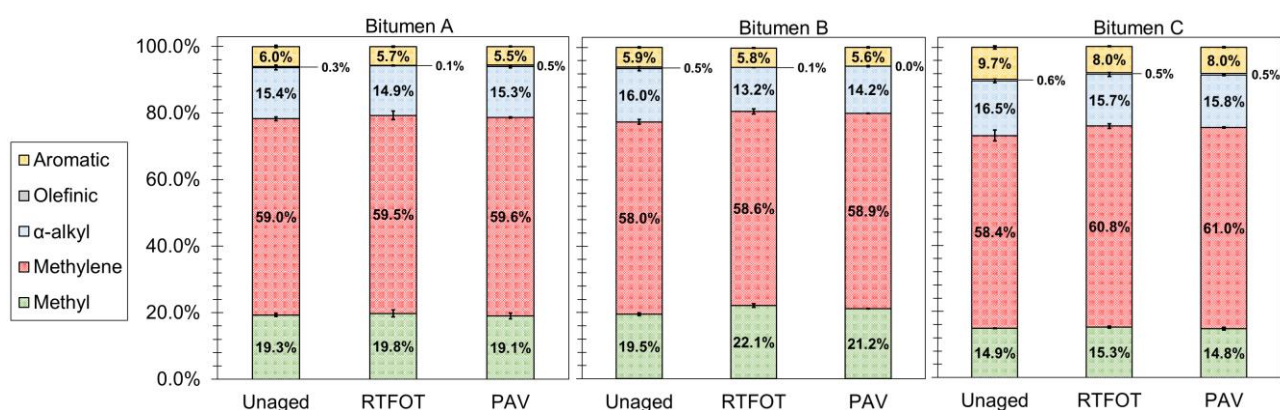
274 Spectroscopic ¹H-NMR analyses were evaluated to gain insights into possible changes of proton distribution upon
 275 ageing and thus the chemical composition of bitumens. An inspection of the spectra in all the ageing states for bitumen
 276 A (Figure 3) revealed a large peak at 0.90 ppm assigned to alkyl (methyl) protons and a peak at 1.28 ppm related to alkyl
 277 (methylene) protons, something which was observed also for binders B and C. After long term-ageing with PAV, bitumen
 278 A showed a peak around 1.67 ppm ascribed to alkyl (methine) protons. The same peak was observed already for B-
 279 RTFOT and C-RTFOT with the intensity of the peak increasing after PAV. The broader peak between 2.00-2.30 ppm can
 280 be assigned to protons on C_α next to carbonyl and the peak at 2.30 ppm can be assigned to a benzylic proton. No significant
 281 peaks were observed in the olefinic proton region (4.00-6.00 ppm) in any of the ageing states. The broader signal from
 282 6.50 to 8.50 ppm is related to the aromatic protons.

283 Although spectral peaks appear somewhat similar apart from the prominent peak at 1.67 ppm upon ageing, integration
 284 of specific regions given in Table 2 (for which relative percentage distribution was determined) allows for the discussion
 285 of the chemical alterations upon standardised ageing. The relative occurrence of protons in different chemical
 286 environments/ageing states is given in Figure 11. All the analysed samples present a negligible presence of olefinic
 287 protons independent of the bitumen's ageing state. For clarity the standard deviations of this specific region are not
 288 presented, whereas standard deviations of all the other regions are included in Figure 11. In bitumens A and B, the
 289 governing region seems to be the methylene, followed by methyl, α-alkyl and aromatic proton regions, while for bitumen

290 C the methyl and α -alkyl region appeared in different decreasing percentage order. The main differences between bitumen
 291 A and B are the lower methyl region and the higher methylene region for bitumen A. Since methylene is the region that
 292 contributes predominantly in the total spectral region of the aliphatic protons ($=H_{\text{methylene}}+H_{\text{methyl}}+H_{\alpha\text{-alkyl}}$) its lower
 293 percentage for bitumen B is reasonable based on the different distillation grade of the two bitumens. As mentioned
 294 previously in the limitations of each spectroscopic technique, $^1\text{H-NMR}$ can capture only molecules containing protons,
 295 and this should always be taken into account when fractionation is considered as with this technique the total bitumen
 296 composition is missing. In addition, bitumens A and B differ from bitumen C mainly by the lower fraction in the aromatic
 297 and the higher fraction in the methyl regions.

298 The effect of the ageing state with regard to the relative percentage of protons was also assessed and presented in
 299 Figure 11. More specifically, in the hard bitumen A, the methylene proton region appears to increase slightly from 59.0%
 300 in A-Unaged to 59.5% in A-RTFOT and remains constant in A-PAV (59.6%). The aromatic protons follow the opposite
 301 trend (6.0% for A-Unaged to 5.5% for A-PAV). The region linked with the methyl protons fluctuated for bitumen A
 302 (19.3% - A-Unaged, 19.8% - A-RTFOT, 19.1% - A-PAV).

303



304

305 Figure 11: Percentage distribution of protons in different ageing states of bitumen A, B and C as determined by $^1\text{H NMR}$.

306

307 Bitumen B originating from the same crude oil presents a similar relative percentage proton distribution after
 308 laboratory short- and long-term ageing. It is interesting that the α -alkyl proton zone from 16.0% in B-Unaged decreased
 309 in B-RTFOT (13.2%) and PAV (14.2%) compared to the unaged state. A fluctuation for the methyl protons was observed
 310 for bitumen B (increased percentage after RTFOT and decreased percentage values upon PAV), a trend which was
 311 observed also for bitumen A. Changes in the methylene proton region showed also an upward relative percentage trend
 312 with ageing.

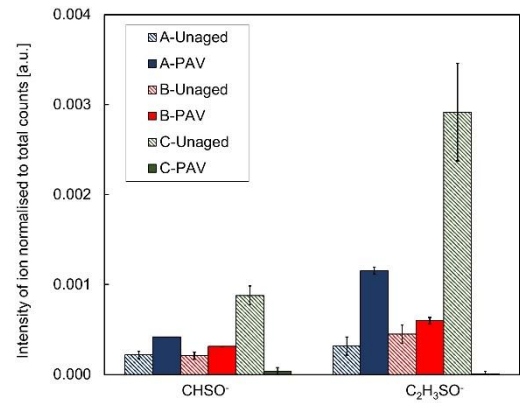
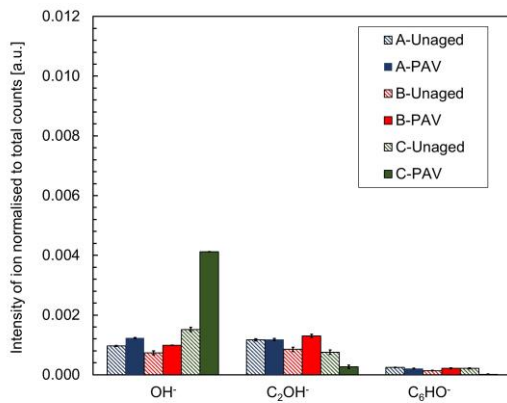
313 Bitumen C, which gave the most apparent difference in the FTIR and the EPR results, showed a different initial proton
314 relative percentage distribution compared to A and B-Unaged (higher aromatic and α -alkyl proton percentages, lower
315 methyl proton percentages) but demonstrated, in general, the same trends with ageing. More specifically, bitumen C
316 showed a decreasing trend after short-term ageing with RTFOT for the α -alkyl proton region shifting respectively from
317 16.5% in the C-Unaged to 15.7% in C-RTFOT and in 15.8% in the C-PAV, something which was observed also for
318 bitumen B. Similar to bitumens A and B, increasing trends in the methylene and methyl proton regions of bitumen C was
319 also observed, with the methyl proton region increasing with RTFOT ageing. The aromatic region appeared to decrease
320 with ageing for bitumen C.

321 Obstacles of exploratory studies to identify chemical differences upon ageing were overcome by grouping the main
322 proton categories, acknowledging always the limitations that may exist for the application of this technique to bitumen.
323 Therefore, bitumen A and B exhibited in general similar relative percentage distribution of protons as expected for the
324 same crude oil in the unaged state but also upon laboratory ageing where the percentage distribution of protons was quite
325 similar. In addition, the formation of polycyclic aromatics due to the aromatisation process is not expected to be captured
326 with $^1\text{H-NMR}$ since they do not contain a hydrogen in the middle and the relative decrease of this region for bitumen A
327 and C can be possibly attributed to the risk of precipitation due to aromatics condensation with ageing.

328 **3.1.4. TOF-SIMS oxygenated fragments**

329 Molecular investigation of the oxygenated products after the combined effect of short- and long-term ageing was
330 conducted with TOF-SIMS on the surface of the three bituminous samples. Ageing may affect the compatibility of the
331 wax present in bitumen C to appear more pronounced upon ageing in the surface of the films. Although clear differences
332 cannot be seen between the different ageing states *i.e.* in the spectra of bitumen A (Figure 4), a thorough inspection of
333 certain fragment ions assisted to form a more clear view for the products. M/z values in the negative ion spectra of all the
334 bituminous tested samples were classified in groups of ion fragments with generic formulas RSO_x and RHO_x given in
335 Table 3. Selected m/z values in the positive ion spectra were assigned to aromatic and aliphatic ion fragments (Table 3).

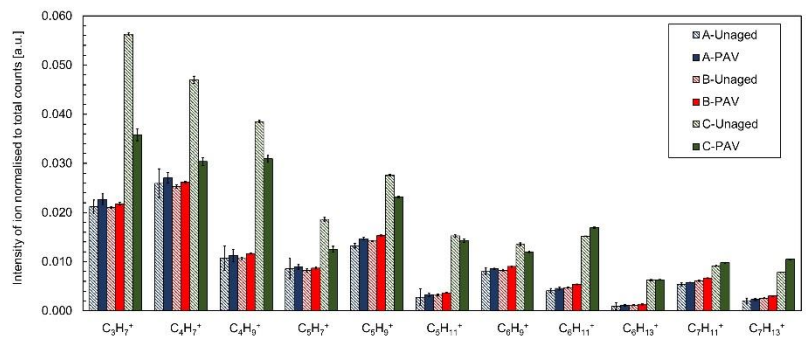
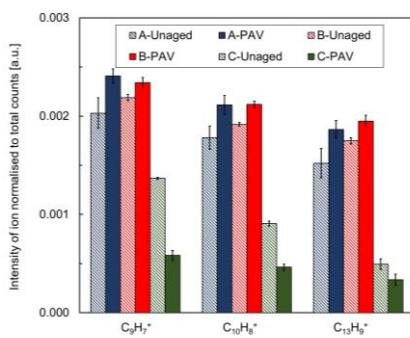
336 The findings of the $(\text{OH})_x$ -containing fragments of bitumen A and B and partially for bitumen C point out that other
337 products such as alcohols/ethers or carboxylic acids can be formed. This is evident by the higher intensity of most of the
338 $(\text{OH})_x$ -containing fragments (attributed possibly to alcohols) after PAV compared to the unaged state which was not
339 observed for specific ion fragments (C_2OH^+ , C_6OH^+) of bitumen C (Figure 12), most probably as a result of the prominent
340 presence of wax in its surface.



341 Figure 12: Intensity of $(OH)_x$ -containing compounds in all the ageing states.
342

Figure 13: Intensity of SO_x -containing compounds in all the ageing states.

343 Similar trends follow for the increase of the ion fragments with generic formula RSO_x given in Figure 13. The results
344 of bitumen A and B support the formation of considerable amounts of sulfoxide-containing compounds after the
345 sequential short and long-term ageing as the intensities of A-PAV and B-PAV remain higher than the unaged state.
346 Caution should always be taken concerning the specific sulfoxide-containing fragments observed with TOF-SIMS which
347 give a partial view of the total sulfoxides present in bitumen which FTIR might capture in a greater penetration depth;
348 this means that limitations should be again acknowledged when comparing the different techniques. Potentially, the results
349 of the two surface techniques could be used to exploit the surface effects of oxidation in bituminous films. Bitumen C
350 seems to reduce the sulfoxide-containing ion fragments with ageing something which does not agree with the FTIR
351 results. This may be explained by the segregation of wax, present in this bitumen, on the surface of the bituminous film,
352 resulting in aliphatic compounds which cover most of the surface [12,52].



353 Figure 14: Intensity of PAH fragments in all the ageing states.

Figure 15: Intensity of aliphatic fragments in all the ageing states.

354 The analysis of selected ions in the positive ion spectra (Figure 14) assigned to polycyclic aromatics hydrocarbons
355 (PAH) is also discussed. The intensity of PAHs of B-Unaged and A-Unaged increased slightly after PAV, whereas a
356 significant drop of PAHs with ageing for bitumen C was captured, probably due to the increase of the waxy particles on

357 the surface upon ageing. Finally, bitumens A and B showed an almost constant behaviour (or a slight increase) of aliphatic
358 ion fragments upon PAV in contrary to bitumen C which showed a decrease for specific aliphatic ion fragments (Figure
359 15). The intensity of the aliphatics for bitumen C appeared the highest a fact that can be explained by the wax present in
360 this binder and the association of wax-related particles with aliphatics on the surface of this bitumen.

361 4. Conclusions

362 This study addressed the main chemical changes that take place in bitumen with standardised laboratory short- and
363 long-term ageing based on advanced spectroscopic techniques. Three binders were investigated, bitumen A and B
364 originating from the same crude source, while bitumen C was obtained from a different source, by a different
365 manufacturing process, and contained natural wax.

366 FTIR supported, in agreement with past literature, the increase of the oxygenated indices of sulfoxide and carbonyl
367 for all binders, independently of bitumen source, distillation process and performance for all the ageing steps. Differences
368 in the extent of carbonyl and sulfoxide formation were observed between the various binders. In FTIR, no clear changes
369 appeared for the aromaticity and branched aliphatic indices with the applied FTIR analysis method. To understand further
370 the formation of the final products, EPR analyses explored the role of organic carbon-centred radicals. These were
371 increased for all three bitumens of different crude source, distillation and empirical properties with short-term ageing and
372 stabilised onwards for the wax-free bitumen A and B, while they slightly decreased for the waxy, visbroken bitumen C.
373 The EPR VO^{2+} centres remained relatively constant and were almost insusceptible to ageing for all three bitumens,
374 regardless of their crude source or distillation. Additionally, 1H -NMR results showed that the relative distribution of
375 protons is rather unaffected by the ageing steps. Only slight changes were observed, such as an increase in the relative
376 amount of methyl and methylene protons, and a decrease in α -alkyl and aromatic protons. TOF-SIMS managed to reveal
377 a more detailed view of the increase of sulfoxide-containing compounds which were increased significantly after the
378 sequentially short-and long-term ageing for bitumens A and B originating from the same crude source and varying only
379 in empirical properties. For the waxy, visbroken bitumen C originating from a different crude source, the presence of wax
380 affected the surface molecular characterisation reporting a decrease for most of the SO_x - and $(OH)_x$ -containing fragments.
381 The $(OH)_x$ -containing fragments suggested that apart from carbonyls, other products such as alcohols and carboxylic
382 acids can be produced.

383 Since each technique has its specific limitations, the results from different techniques may sometimes seem conflicting
384 and should be interpreted carefully. Moreover, some of the test methods are typical surface/interface techniques with
385 different penetration depths, such as TOF-SIMS and FTIR, while for others, *i.e.* liquid 1H -NMR, the sample needs to be
386 dissolved in a solvent. These different parameters may have an effect on the results.

387 In summary, this work reported the oxygenated intermediate and final products in bitumen and provided some
388 experimental insights in order to understand better the oxidative mechanisms that could occur in bitumen besides the
389 well-reported sulfoxide and carbonyl formation. In the future, a comparison between the ageing mechanisms of bitumen
390 after laboratory ageing with the mechanisms of field aged bitumen is proposed to be performed in order to understand
391 whether similar changes in bitumen chemistry take place in field conditions.

392 Acknowledgements

393 The authors gratefully acknowledge the technical assistance by Jimmy Matheussen from Bureau Veritas, Pieter
394 Mampuy (ORSY) and Glenn Van Haesendonck (BAMS) from the University of Antwerp, as well as support from Nynas
395 AB and the European Union for H.Y. Vincent Ching's H2020-MSCA-IF grant (grant number 792946. iSPY).

396

397 References

- 398 [1] J.S. Moulthrop, M. Massoud, The SHRP Materials Reference Library, Washington DC, 1993.
- 399 [2] P.E.Y. Wang, Y. Wen, K. Zhao, D. Chong, A.S.T. Wong, Evolution and locational variation of asphalt binder
400 aging in long-life hot-mix asphalt pavements, *Constr. Build. Mater.* 68 (2014) 172–182.
401 <https://doi.org/10.1016/j.conbuildmat.2014.05.091>.
- 402 [3] F. Wang, Y. Xiao, P. Cui, J. Lin, M. Li, Z. Chen, Correlation of asphalt performance indicators and aging
403 Degrees : A review, *Constr. Build. Mater.* 250 (2020) 118824.
404 <https://doi.org/10.1016/j.conbuildmat.2020.118824>.
- 405 [4] X. Lu, U. Isacson, Effect of ageing on bitumen chemistry and rheology, *Constr. Build. Mater.* 16 (2002) 15–22.
406 [https://doi.org/10.1016/s0950-0618\(01\)00033-2](https://doi.org/10.1016/s0950-0618(01)00033-2).
- 407 [5] M.C. Cavalli, M. Zaujanis, E. Mazza, M.N. Partl, L.D. Poulikakos, Aging effect on rheology and cracking
408 behaviour of reclaimed binder with bio-based rejuvenators, *J. Clean. Prod.* 189 (2018) 88–97.
409 <https://doi.org/10.1016/j.jclepro.2018.03.305>.
- 410 [6] J.C. Petersen, R. Glaser, Asphalt Oxidation Mechanisms and the Role of Oxidation Products on Age Hardening
411 Revisited, *Road Mater. Pavement Des.* 12 (2011) 795–819. <https://doi.org/10.1080/14680629.2011.9713895>.
- 412 [7] X. Hou, F. Xiao, J. Wang, S. Amirhanian, Identification of asphalt aging characterization by spectrophotometry
413 technique, *Fuel.* 226 (2018) 230–239. <https://doi.org/10.1016/j.fuel.2018.04.030>.
- 414 [8] A.A.A. Molenaar, E.T. Hagos, M.F.C. van de Ven, Effects of Aging on the Mechanical Characteristics of
415 Bituminous Binders in PAC, *J. Mater. Civ. Eng.* 22 (2010). [https://doi.org/10.1061/\(ASCE\)MT.1943-5533.0000021](https://doi.org/10.1061/(ASCE)MT.1943-5533.0000021).
- 417 [9] J.C. Petersen, A Review of the Fundamentals of Asphalt Oxidation (E-C140), *Transp. Res. Rec. J. Transp. Res.*
418 *Board.* (2009). <https://doi.org/10.17226/23002>.
- 419 [10] The Shell Bitumen Handbook, 6th edition, ICE Publishing, 2015. <https://doi.org/10.1680/tsbh.58378>.
- 420 [11] L. Loebera, G. Muller, J. Morel, O.C. Sutton, L. Havre, L. Havre, Bitumen in colloid science : a chemical ,
421 structural and rheological approach, 77 (1998) 1443–1450.
- 422 [12] G. Pipintakos, H.Y.V. Ching, H. Soenen, P. Sjövall, U. Mühlich, S. Van Doorslaer, A. Varveri, W. Van den
423 bergh, X. Lu, Experimental investigation of the oxidative ageing mechanisms in bitumen, *Constr. Build. Mater.*
424 260 (2020) 119702. <https://doi.org/10.1016/j.conbuildmat.2020.119702>.
- 425 [13] P. Herrington, B. James, T.F.P. Henning, Validation of a Bitumen Oxidation Rate Model, *Transp. Res. Rec. J.*
426 *Transp. Res. Board.* 2632 (2017) 110–118. <https://doi.org/10.3141/2632-12>.
- 427 [14] U. Mühlich, G. Pipintakos, C. Tsakalidis, Mechanism based diffusion-reaction modelling for predicting the
428 influence of SARA composition and ageing stage on spurt completion time and diffusivity in bitumen, 267 (2021).
429 <https://doi.org/10.1016/j.conbuildmat.2020.120592>.
- 430 [15] J. Petersen, P. Harnsberger, Asphalt Aging: Dual Oxidation Mechanism and Its Interrelationships with Asphalt
431 Composition and Oxidative Age Hardening, *Transp. Res. Rec. J. Transp. Res. Board.* 1638 (1998) 47–55.
432 <https://doi.org/10.3141/1638-06>.
- 433 [16] P.R. Herrington, Thermal decomposition of asphalt sulfoxides, *Fuel.* 74 (1995) 1232–1235.
- 434 [17] SHRP-A-370, Binder Characterization and Evaluation Volume 4: Test Methods, n.d.
- 435 [18] L.D. Poulikakos, C.F. A, D. Wang, L. Porot, B. Hofko, Impact of asphalt aging temperature on chemomechanics,
436 *RSC Adv.* 9 (2019) 11602–11613. <https://doi.org/10.1039/C9RA00645A>.

- 437 [19] B. Hofko, L. Porot, A.F. Cannone, L. Poulikakos, L. Huber, X. Lu, H. Grothe, K. Mollenhauer, FTIR spectral
438 analysis of bituminous binders : reproducibility and impact of ageing temperature, *Mater. Struct.* 51 (2018).
439 <https://doi.org/10.1617/s11527-018-1170-7>.
- 440 [20] D. Lesueur, A. Teixeira, M.M. Lázaro, D. Andaluz, A. Ruiz, A simple test method in order to assess the effect of
441 mineral fillers on bitumen ageing, *Constr. Build. Mater.* 117 (2016) 182–189.
442 <https://doi.org/10.1016/j.conbuildmat.2016.05.003>.
- 443 [21] EN12607-1: Bitumen and bituminous binders. Determination of the resistance to hardening under the influence
444 of heat and air–Part 1: RTFOT method, 2007.
- 445 [22] EN 14769: Bitumen and Bituminous Binders. Accelerated Long-term Ageing Conditioning by a Pressure Ageing
446 Vessel (PAV), 2012.
- 447 [23] K. Zhao, Y. Wang, F. Li, Influence of ageing conditions on the chemical property changes of asphalt binders,
448 *Road Mater. Pavement Des.* (2019) 1–29. <https://doi.org/10.1080/14680629.2019.1637771>.
- 449 [24] F. Liu, Z. Zhou, X. Zhang, Y. Wang, On the linking of the rheological properties of asphalt binders exposed to
450 oven aging and PAV aging, *Int. J. Pavement Eng.* 0 (2019) 1–10.
451 <https://doi.org/10.1080/10298436.2019.1608992>.
- 452 [25] N.A. Al-azri, S.H. Jung, K.M. Lunsford, A. Ferry, J.A. Bullin, R.R. Davison, C.J. Glover, Binder Oxidative Aging
453 in Texas Pavements Hardening Rates , Hardening Susceptibilities , and Impact of Pavement Depth, (n.d.) 12–20.
- 454 [26] C.H. Domke, R.R. Davison, C.J. Glover, Effect of Oxygen Pressure on Asphalt Oxidation Kinetics RT), (2000)
455 592–598. <https://doi.org/10.1021/ie9906215>.
- 456 [27] Y. Li, S. Wu, Q. Liu, Y. Dai, C. Li, H. Li, S. Nie, Aging degradation of asphalt binder by narrow-band UV
457 radiations with a range of dominant wavelengths, *Constr. Build. Mater.* 220 (2019) 637–650.
458 <https://doi.org/10.1016/j.conbuildmat.2019.06.035>.
- 459 [28] J. Mirwald, D. Maschauer, B. Hofko, H. Grothe, Impact of reactive oxygen species on bitumen aging – The
460 Viennese binder aging method, *Constr. Build. Mater.* 257 (2020) 119495.
461 <https://doi.org/10.1016/j.conbuildmat.2020.119495>.
- 462 [29] P.R. Herrington, Diffusion and reaction of oxygen in bitumen films, *Fuel.* 94 (2012) 86–92.
463 <https://doi.org/10.1016/j.fuel.2011.12.021>.
- 464 [30] A. Dony, L. Ziyani, I. Drouadaine, S. Pouget, S. Faucon-Dumont, D. Simard, V. Mouillet, J.E. Poirier, T. Gabet,
465 L. Boulange, A. Nicolai, C. Gueit, 1, MURE National Project : FTIR spectroscopy study to assess ageing of
466 asphalt mixtures, in: 6th Eurasphalt Eurobitume Congr., 2016. <https://doi.org/10.14311/EE.2016.154>.
- 467 [31] R. Tauste, Understanding the bitumen ageing phenomenon : A review, *Constr. Build. Mater.* 192 (2018) 593–
468 609. <https://doi.org/10.1016/j.conbuildmat.2018.10.169>.
- 469 [32] F.J. Ortega, F.J. Navarro, M. Jasso, L. Zanzotto, Physicochemical softening of a bituminous binder by a reactive
470 surfactant (dodecyl succinic anhydride , DSA), *Constr. Build. Mater.* 222 (2019) 766–775.
471 <https://doi.org/10.1016/j.conbuildmat.2019.06.117>.
- 472 [33] J. Lamontagne, P. Dumas, V. Mouillet, J. Kister, Comparison by Fourier transform infrared (FTIR) spectroscopy
473 of different ageing techniques : application to road bitumens, *Fuel.* 80 (2001) 483–488.
474 [https://doi.org/10.1016/S0016-2361\(00\)00121-6](https://doi.org/10.1016/S0016-2361(00)00121-6).
- 475 [34] A. Stoll , S.; Schweiger, EasySpin, a comprehensive software package for spectral simulation and analysis in
476 EPR, *J. Magn. Reson.* 178 (2006) 42–55. <https://doi.org/10.1016/j.jmr.2005.08.013>.
- 477 [35] M. Espinosa; P.A. Camper; R. Salcedo, Electron Spin Resonance and Electronic Structure of Vanadyl–Porphyrin
478 in Heavy Crude Oils, *Inorg. Chem.* 40 (2001) 4543–4549. <https://doi.org/10.1021/ic000160b>.
- 479 [36] L.G. Gilinskaya, EPR spectra of V(IV) complexes and the structure of oil porphyrins, *J. Struct. Chem.* 49 (2008)
480 245–254. <https://doi.org/10.1007/s10947-008-0120-6>.
- 481 [37] N.S. Ramachandran, Vasanth; van Tol, Johan; McKenna, Amy M.; Rodgers, Ryan P. ; Alan G. Marshall, Ryan
482 P. ; Dalal, High Field Electron Paramagnetic Resonance Characterization of Electronic and Structural
483 Environments for Paramagnetic Metal Ions and Organic Free Radicals in Deepwater Horizon Oil Spill Tar Balls,
484 *Anal. Chem.* 87 (2015) 2306–2313. <https://doi.org/10.1021/ac504080g>.
- 485 [38] N. Nciri, N. Kim, N. Cho, Chemical Characterization of Gilsonite Bitumen Chemical Characterization of
486 Gilsonite Bitumen, (2014). <https://doi.org/10.4172/2157-7463.1000193>.
- 487 [39] J.C. Poveda, D.R. Molina, Journal of Petroleum Science and Engineering Average molecular parameters of heavy
488 crude oils and their fractions using NMR spectroscopy, *J. Pet. Sci. Eng.* 84–85 (2012) 1–7.
489 <https://doi.org/10.1016/j.petrol.2012.01.005>.
- 490 [40] L. J. O’Neil, P.E. Heckelman, C.B. Koch, K.J. Roman, The Merck Index, an Encyclopedia of Chemicals, Drugs,
491 and Biologicals, Merck Research Laboratories; 14th Edition, 2006.
- 492 [41] C.O. Rossi, P. Caputo, G. De Luca, L. Maiuolo, S. Eskandarsefat, C. Sangiorgi, 1H-NMR Spectroscopy : A

- 493 Possible Approach to Advanced Bitumen Characterization for Industrial and Paving Applications, *Appl. Sci.* 8
494 (2018). <https://doi.org/10.3390/app8020229>.
- 495 [42] V. Thiel, P. Sjövall, Time-of-Flight Secondary Ion Mass Spectrometry (TOF-SIMS): Principles and Practice in
496 the Biogeosciences, in: *Princ. Pract. Anal. Tech. Geosci.*, Royal Society of Chemistry, 2015: pp. 122–170.
- 497 [43] X. Lu, P. Sjövall, H. Soenen, Structural and chemical analysis of bitumen using time-of-flight secondary ion mass
498 spectrometry (TOF-SIMS), *Fuel.* 199 (2017) 206–218. <https://doi.org/10.1016/j.fuel.2017.02.090>.
- 499 [44] A.M. Hung, A. Goodwin, E.H. Fini, Effects of water exposure on bitumen surface microstructure, *Constr. Build.
500 Mater.* 135 (2017) 682–688. <https://doi.org/10.1016/j.conbuildmat.2017.01.002>.
- 501 [45] J. Blom, H. Soenen, A. Katsiki, N. Van Den Brande, H. Rahier, Investigation of the bulk and surface
502 microstructure of bitumen by atomic force microscopy, *Constr. Build. Mater.* 177 (2020) 158–169.
503 <https://doi.org/10.1016/j.conbuildmat.2018.05.062>.
- 504 [46] A. Ramm, M.C. Downer, N. Sakib, A. Bhasin, Morphology and kinetics of asphalt binder microstructure at gas,
505 liquid and solid interfaces., *J. Microsc.* 276 (2019) 109–117. <https://doi.org/10.1111/jmi.12842>.
- 506 [47] H. Soenen, X. Lu, O.-V. Laukkanen, Oxidation of bitumen: molecular characterization and influence on
507 rheological properties, *Rheol. Acta.* 55 (2016) 315–326. <https://doi.org/10.1007/s00397-016-0919-6>.
- 508 [48] G. Tarsi, A. Varveri, C. Lantieri, A. Scarpas, C. Sangiorgi, Effects of Different Aging Methods on Chemical and
509 Rheological Properties of Bitumen, *J. Mater. Civ. Eng.* 30 (2018). [https://doi.org/10.1061/\(asce\)mt.1943-5533.0002206](https://doi.org/10.1061/(asce)mt.1943-5533.0002206).
- 510
- 511 [49] I. Gabrielle do Nascimento Camargo, B. Hofko, J. Mirwald, G. Hinrich, Effect of Thermal and Oxidative Aging
512 on Asphalt Binders Rheology and Chemical Composition, *Materials (Basel).* 13 (2020) 4438.
513 <https://doi.org/doi:10.3390/ma13194438>.
- 514 [50] J.F. Branham, J.C. Petersen, R.E. Robertson, J.J. Duvall, S.S. Kim, P.M. Harnsberger, T. Mill, E.K. Ensley, F.A.
515 Barbour, J.F. Schabron, SHRP-A-368 Binder Characterization and Evaluation Volume 2: Chemistry,
516 Washington, DC, 1993.
- 517 [51] J.H. Tannous, A. De Klerk, Quantification of the Free Radical Content of Oilsands Bitumen Fractions, *Energy &
518 Fuels.* 33 (2019) 7083–7093. <https://doi.org/10.1021/acs.energyfuels.9b01115>.
- 519 [52] X. Lu, P. Sjövall, H. Soenen, M. Andersson, Microstructures of bitumen observed by environmental scanning
520 electron microscopy (ESEM) and chemical analysis using time-of- flight secondary ion mass spectrometry (
521 TOF-SIMS), *Fuel.* 229 (2018) 198–208. <https://doi.org/10.1016/j.fuel.2018.05.036>.